Optimal Source Distribution for Hyperthermia at the Center of a Sphere of Muscle Tissue

CAREY M. RAPPAPORT, MEMBER, IEEE, AND FREDERIC R. MORGENTHALER, FELLOW, IEEE

Abstract—**In noninvasive electromagnetic hyperthermia it is important that applicators deposit as least as much power at the tumor as anywhere else in the intervening tissue. This study determines the ideal penetration limits for heating the center of a volume of muscle tissue according to this constraint. First, it is shown that the most efficiently heated volume is a sphere. Then, using both a diffraction integral formulation and a spherical harmonic modal approach, field distributions within the sphere are derived. It is shown that combining odd harmonics can generate a nearly uniform surface power distribution, and that this distribution is optimal. The power deposition patterns for these distributions for various standard frequencies are presented. It is concluded that 915 MHz is the best frequency for heating spheres less than 9.5 cm in radius.**

I. Introduction

THE USE OF microwaves to induce hyperthermia by depositing power within biological tissue is an effective means of treating cancer [1]–[3]. Applied noninvasively, microwave radiation is relatively safe and controllable, and may be synergistically combined with ionizing radiation or chemotherapy.

It is important to know the penetration depth limits which produce local power maxima. For treatment which provides heat at depth at the site of a localized, solid tumor, overheating normal intervening tissue must be avoided. The greatest depth for which power can be safely deposited occurs in a spherical volume of tissue. Also, with proper focusing, this penetration depth represents a fundamental heating limit.

In contrast to several previously reported studies, the current examination considers the synthesis of the particular best distribution. A large amount of work has been done analyzing the power pattern in a sphere illuminated by a plane wave [4]–[6]. For this scattering problem, the deposition pattern is unsymmetrical, since power is incident from only one side. Placing sources on all sides—in effect surrounding the sphere with sources—makes use of the entire apperture and therefore provides the greatest constructive interference at the center. The symmetric distribution synthesized has a much greater focal-point-to-surface distance than the plane wave pattern. The optimal synthesis problem, though conceptually more complex, is less computationally difficult than the plane wave scattering analysis, which is usually solved using numerical approximations. Since the former specifies a source polarization, phase, and amplitude distribution on the sphere surface, it is not easily analyzed using ray paths or wavefronts. However, since the solution is ultimately determined in terms of spherical harmonics, it is specified in closed form.

There are relatively few biological structures which can be modeled by the spherical geometry. The head (with adequate eye protection) and the breast, making use of the higher conductivity muscle "ground plane" backing layer, are possible candidates. Despite the limited applications, however, knowledge of the absolute maximum heating depth provides a rule of thumb which specific microwave applicator designs might strive to approach, but never exceed.

II. Lossy Sphere Field Solutions

Since attenuation in dissipative media is roughly exponential with depth, the volume geometry most suitable for maximum constructive interference is one which minimizes the distance from a focal point to the source on its surface. By this criterion a sphere is optimum, since any other volume can always be inscribed by a sphere. Thus, given the minimum focal-point-to-surface distance R, and the maximum tolerable surface power, a sphere of radius R will yield the greatest power maximum at that focal point, the origin.

The polarization of the source on the surface of the sphere is an important criterion. As shown in Fig. 1, it must be parallel to some axis, say the z axis. By symmetry, these z-directed source components are independent of circulating angle (ϕ), and have polar angle (θ) dependence which is symmetric about the equator ($\theta = \pi/2$). Any additional radially symmetric (r) polarization component cancels itself at the center, whereas any circulating component vanishes there, and any additional polar angle component can be decomposed into a radial component and a z-directed component. If possible, a source design should maintain polarization parallel to the z axis.

Specifying the optimal phases and amplitudes of these source components is the next step in this derivation. Contrary to established intuition, the best focused source

Manuscript received April 6, 1987; revised July 23, 1987. This work was supported in part by the National Institutes of Health under Grant CA 31303.

C. M. Rappaport was with the Department of Electrical Engineering and Computer Science, Massachusetts Institute of Technology, Cambridge, MA 10239. He is now with the Department of Electrical Engineering, Northeastern University, Boston, MA.

F. R. Morgenthaler is with the Department of Electrical Engineering and Computer Science, Massachusetts Institute of Technology, Cambridge, MA 01239.

IEEE Log Number 8717113.

0018-9480/87/1200-1322$01.00

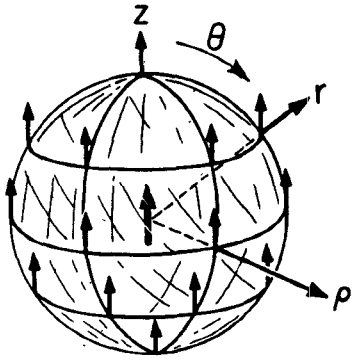

Fig. 1. Currents polarized in the z direction on the surface of a sphere, and the resulting maximum constructive interference of electric field at the center.

distribution is not uniform amplitude and phase, as it would be for an acoustic compression wave. To examine the deficiencies of this uniform distribution, we first solve the surface current diffraction integral, and then improve this solution using a modal analysis to yield the optimum distribution.

The uniform z-polarized surface current at a radius R is represented as $J(r') = \delta(r - R)\hat{z}$., where δ is the spatial impulse function. This current is inserted in the dyadic Green's function diffraction formula [7]

$$E = -j\omega\left(\bar{\bar{I}} + \frac{1}{k^2}\nabla\nabla\right)\cdot A(r) \tag{1}$$

$$A(r) = \mu\int_{V'} dv' \frac{e^{-jk|r-r'|}}{4\pi|r-r'|}J(r') \tag{2}$$

where the left-hand side of (1) is the vector electric field at the observer point r, $A(r)$ is the vector potential, ω is the radian frequency, $\bar{\bar{I}}$ is the dyadic identity, $k = \beta - j\alpha$ is the complex wavenumber, and $|r - r'|$ is the observer-to-integration-point distance. The law of cosines is used to represent $|r - r'|$, where r is assumed to lie on the z axis. This alignment assumption is justified since the source is uniform and symmetric and the only requirement on polarization is that it be parallel to any arbitrary axis. That is, the vector potential A is independent of observer coordinates θ and ϕ. As would be the case with a scalar wave, A represents a family of concentric, spherical equipotentials. The source polarization enters only as a linear multiplier to this scalar function. The integral in (2) becomes a surface integral:

$$A(r) = \mu\int_0^{\pi} d\theta' \int_0^{2\pi} d\phi' R^2 \sin\theta' \frac{e^{-jk\sqrt{R^2 + r^2 - 2rR\cos\theta'}}}{4\pi\sqrt{R^2 + r^2 - 2rR\cos\theta'}}\hat{z} \tag{3}$$

which is readily integrated, giving

$$A = \hat{z}\frac{\mu}{2}\left(\frac{R}{-jkr}\right)\left(e^{-jk|R+r|} - e^{-jk|R-r|}\right). \tag{4}$$

Inside the sphere, $r < R$, the vector potential can be represented by a spherical Bessel function:

$$A(r) = \hat{z}\mu R e^{-jkR}\frac{\sin kr}{kr} = \hat{z}\mu R e^{-jkR} j_0(kr). \tag{5}$$

It is at this point that the vector nature of the electromagnetic field presents itself. Substituting this expression back into (1) and taking derivatives in cylindrical coordinates (ρ, ϕ, z) gives

$$E(z,\rho) = -j\omega\mu R e^{-jkR}\left\{\hat{z}\left[\left(\frac{\rho}{r}\right)^2\left(j_0(kr) - \frac{j_1(kr)}{kr}\right) + \left(\frac{z}{r}\right)^2\left(2\frac{j_1(kr)}{kr}\right)\right] + \hat{\rho}\left(\frac{z\rho}{r^2}\right)\left[-j_0(kr) + 3\frac{j_1(kr)}{kr}\right]\right\} \tag{6}$$

with $r = \sqrt{z^2 + \rho^2}$.

Several features of (6) are worth mentioning. First, there is the addition of the $\hat{\rho}$ component, and the $\hat{z}$ component has three terms instead of just one (as might be expected for a scalar field). Second, for small values of radius, since $j_0(kr) \sim 1$ and $j_1(kr) \sim kr/3$, the electric field reduces to simply

$$E(z,\rho) \approx -\hat{z}j\omega\mu R e^{-jkR}\left(\tfrac{2}{3}\right) \approx \hat{z}\left(-j\tfrac{2}{3}\right)\eta k R e^{-jkR}. \tag{7}$$

Next, for large values of radius $|j_n(kr)| \sim |\sin(kr + \frac{n\pi}{2})/kr|$, so (6) becomes

$$E(z,\rho) \approx -j\eta k R e^{-jkR} j_0(kr)\frac{\rho}{r}\left(\hat{z}\frac{\rho}{r} - \hat{\rho}\frac{z}{r}\right). \tag{8}$$

Note that in (8) there is an appreciable E_ρ component away from the equator. Thus even though the surface currents are polarized parallel to the z axis, it is recognized that the resulting E field for large radii is primarily polarized in the θ direction.

The dissipated power in a medium of conductivity σ is $\frac{\sigma}{2}|E|^2$. From (8), this is seen to be

$$P(z,r) = \frac{\sigma\eta^2}{2}|kR|^2 e^{-2\alpha R}|j_0(kr)|^2\left(\frac{\rho}{r}\right)^2 \tag{9}$$

which is maximized at $z = 0$, $\rho = r$, at the equator. The exact power deposition function, based on (6) normalized to the power at the origin, is plotted as a function of radius at $z = 0$ in Fig. 2 for several standard microwave hyperthermia frequencies [8]. It is the intersection of each curve with unity which determines the maximum allowable sphere radius. As would be expected, the lowest frequency curve has a greater penetration depth, due to its larger physical wavelength, whereas the higher frequency patterns have much greater resolution, with a rather narrow peak at the origin for 2450 MHz. An interesting anomaly exists for 915 MHz, where the penetration depth is actually greater than 433 MHz. This is due to the more prominent

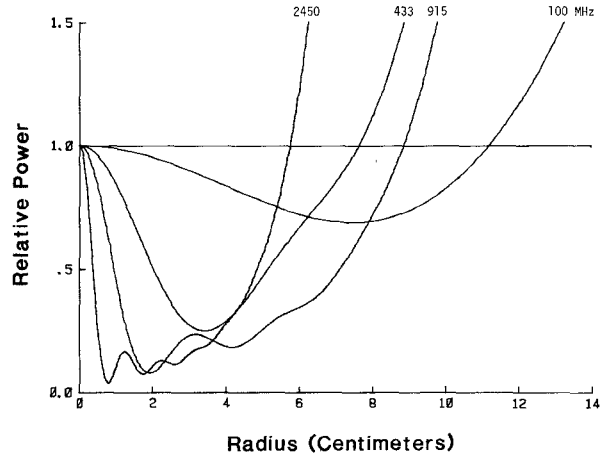

Fig. 2 Dissipated power in a sphere of muscle tissue as a function of radius at $\theta = \pi/2$ for four standard hyperthermia frequencies: uniform current distribution

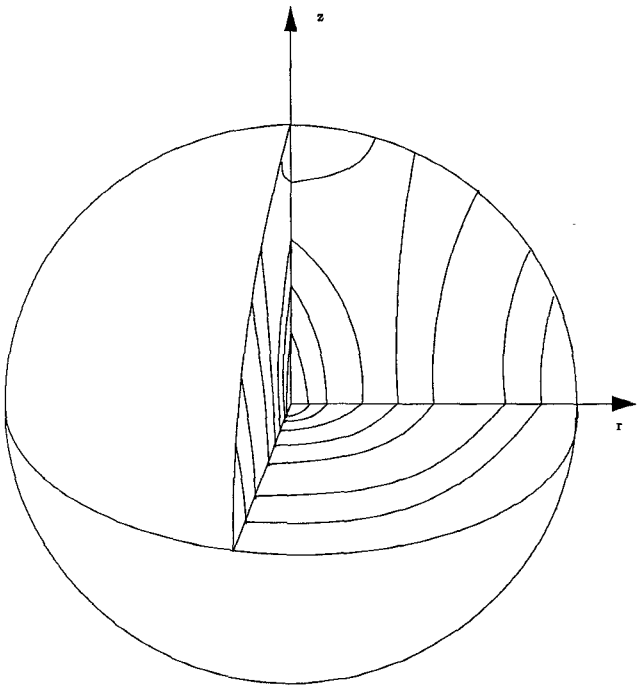

Fig. 3. Power contours within a sphere of muscle tissue illuminated with a uniform phase and amplitude, vertically polarized current source.

constructive and destructive phase effects for the higher frequency.

Fig. 3 schematically represents the power contours within the sphere. The profile of Fig. 2 is plotted along the horizontal radial line from the center.

For a given (large) radius, (9) shows that the power varies as $\sin^2\theta$. This is the same angular dependence as the far-field power flow of a Hertzian dipole, resulting from the $\sin\theta$ factor in the transverse component of the E field and the H field. Much more power is deposited at the equator than at regions near the poles. It is this inbalance which is corrected using modal analysis in the next section to yield the optimum vector wave solution to the power deposition problem.

Testing the large radius assumption for (8) with the worst case, 433 MHz, where the maximum radius is approximately 0.9λ, $|kr| = 6.3$ results in the neglected power being only of the order of 0.04 at $\rho = 0$. For 915 MHz, this error is only about 1 percent.

III. Modal Analysis

Solutions to the wave equation for spherical geometry are harmonics of index n, represented by [9]:

$$\begin{aligned} \boldsymbol{E}(\boldsymbol{r}) = \sum_{n=1}^{N} & \hat{r}A_n \frac{n(n+1)}{kr} j_n(kr) P_n(\cos\theta) \\ & + \hat{\theta}A_n \left[j_{n-1}(kr) - \frac{n}{kr} j_n(kr) \right] \\ & \times \left[n\cos\theta P_n(\cos\theta) - nP_{n-1}(\cos\theta) \right] \left(\frac{1}{\sin\theta} \right) \end{aligned} \quad (10)$$

where P_n is the Legendre polynomial of order n, and A_n is the constant of the nth harmonic. By setting N equal to 1, $A_1 = -j\omega\mu Re^{-jkR}$, and recalling that $P_0(\cos\theta) = 1$ and $P_1(\cos\theta) = \cos\theta$, it is evident that (6) is the first harmonic spherical wave solution.

It is the fundamental point of this analysis that for higher order harmonics, $n = 2, 3, 4 \cdots$, the E field at $r = 0$ vanishes. Since $j_n(kr)$ varies as $(kr)^n$ for small r, these spherical Bessel functions approach zero at the origin. This property is used to reduce undesirably high power levels at the surface of the sphere without affecting the power at the origin. Specifically, a distribution can be synthesized from these higher order modes with appropriately chosen phase and amplitude to partially cancel the first-order mode field at the surface, near the equator, and thereby increase the maximum sphere size.

Once again, for large radius values, the θ component of the E field is the dominant contribution to the dissipated power function. The θ dependence of the nth mode of E_θ can be expressed as

$$E_{\theta n}(\theta) \sim \hat{\theta} \frac{\partial P_n(\cos\theta)}{\partial(\cos\theta)}. \quad (11)$$

Since for even-order n, $P_n(\cos\theta)$ is an even function of $\cos\theta$, its derivative will be an odd function of $\cos\theta$, with a total value of zero at $\theta = \pi/2$. The goal is to find the harmonics with nonzero values at the equator to be subtracted from the $\sin\theta$ dependence of the first harmonic. Thus only odd-order harmonics are considered.

The derivatives of Legendre polynomials comprising the first three odd harmonics are, from (11),

$$\begin{aligned} E_{\theta 1} &\sim -\sin\theta \\ E_{\theta 3} &\sim -\frac{15}{2}\cos^2\theta\sin\theta + \frac{3}{2}\sin\theta \\ E_{\theta 5} &\sim -\frac{315}{8}\cos^4\theta\cos\theta + \frac{105}{4}\cos^2\theta\sin\theta - \frac{15}{8}\sin\theta \end{aligned} \quad (12)$$

with values -1, $3/2$, and $-15/8$ at $\theta = \pi/2$.

The three equations in (12) can be rewritten in terms of sines of odd multiples of θ:

$$E_{\theta 1} \sim -\sin\theta$$
$$E_{\theta 3} \sim -\frac{15}{8}\sin 3\theta - \frac{3}{8}\sin\theta$$
$$E_{\theta 5} \sim -\frac{315}{128}\sin 5\theta - \frac{105}{128}\sin 3\theta - \frac{30}{128}\sin\theta. \quad (13)$$

The sum of three harmonics may now be represented by

$$f(\theta) = \sin\theta + B_1 \sin 3\theta + B_2 \sin 5\theta \quad (14)$$

where B_1 and B_2 are selected to minimize the maximum value of power, $(f(\theta))^2$, over the domain $0 \leqslant \theta \leqslant \pi$. Solving this transcendental formula interactively yields $B_1 = 0.2365$ and $B_2 = 0.0640$. The resulting surface power variation has three equal peaks of 0.685 at $\theta = 0.294\pi$, 0.5π, and $0.706\ \pi$.

Note that a standard infinite Fourier series composed of higher odd harmonics of the fundamental $\sin\theta$ can produce a square pulse of height $\pi/4$, giving a power of 0.617. However, for any finite sum of Fourier terms, there is always a Gibbs phenomenon at the step edge increasing the amplitude by a factor of about 1.09. This would increase the maximum power to 0.733, which is greater than the previously derived maximum.

What remains is the derivation of the actual mode amplitudes and phases which multiply each harmonic so that their sum equals $f(\theta)$. Define $J_n = A_n[j_{n-1}(kR) - n/kRj_n(kR)]$ as the multiplicative constant of E_θ from (10) for a given sphere radius R. Then using (14) and the three equations (13), the system

$$J_1(-1) + J_3\left(-\frac{3}{8}\right) + J_5\left(-\frac{30}{128}\right) = 1$$
$$J_3\left(-\frac{15}{8}\right) + J_5\left(-\frac{105}{128}\right) = B_1$$
$$J_5\left(-\frac{315}{128}\right) = B_2 \quad (15)$$

is derived. The solution is $J_1 = -0.9509$, $J_3 = -0.1148$, $J_5 = -0.0260$.

Although the third- and fifth-order modes do not contribute to power at the origin of the sphere, the first-order mode is slightly reduced in order to compensate for the $\sin\theta$ terms in these higher modes. Thus the amplitude in the center is reduced to -0.9509 of the uniform current value. Renormalizing the coefficients to $J_1' = 1$, $J_3' = 0.1207$, $J_5' = 0.0288$ compensates for this reduction. The surface power is plotted in Fig. 4, along with the uniform current power. The peak power level is reduced to 0.757 of the single mode power. The magnitude of the ripple is about ± 1.5 percent. Addition of higher order terms would reduce the ripple and lower the maximum surface power slightly. The maximum improvement would be less than 2 percent, and since from Fig. 2 the increase in maximum allowable radius varies approximately logarithmically with power, the minute increase in radius does not justify the additional computational complexity required for seventh- and higher order harmonics.

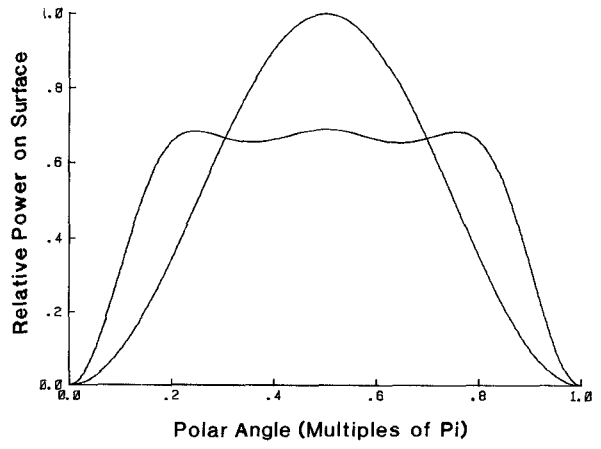

Fig 4. Surface power as a function of θ for single mode (uniform current), and three mode (approximate uniform power) distributions.

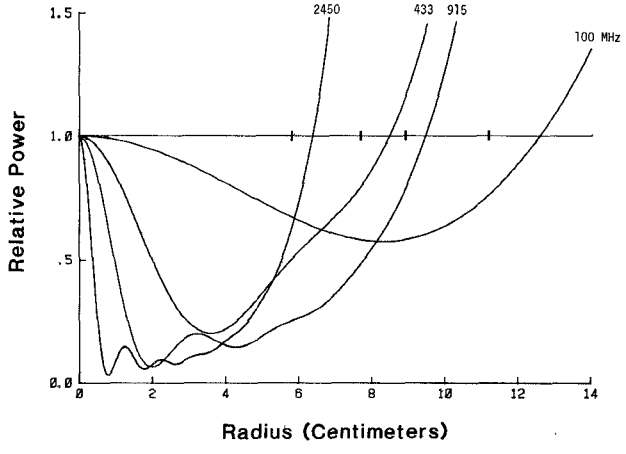

Fig. 5. Power pattern in a sphere of muscle tissue for approximate uniform surface power distribution.

Finally, the coefficients A_n from (10) are determined from the J_n' constants and the magnitudes and phases of the spherical Bessel functions at the unity crossing points of the power pattern for each frequency. Since the pattern changes for each choice of the A_n set, this is an iterative process. For 915 MHz, $A_1 = 1.5e^{j(0.6368)}$, $A_2 = 1.364\ e^{j(-2.8608)}$, and $A_3 = 1.136e^{j(-0.3618)}$, determined at $\beta R = 13.2$, or $R = 9.45$ cm.

The power patterns at $\theta = \pi/2$ for the same frequencies as before are plotted in Fig. 5. Note the increases in maximum allowable radius, as indicated by the intersection points for the uniform current distribution, taken from Fig. 2. For 100, 433, 915, and 2450 MHz, the increases amount to 1.72, 0.84, 0.57, and 0.32 cm, respectively.

From (10), it can be seen that for the large radius dominant E_θ term, the radial and polar angle dependencies are independent. Thus, the radial power behavior always has the same shape as shown in Fig. 5 scaled by the θ dependence of Fig. 4 (with the exception of regions near

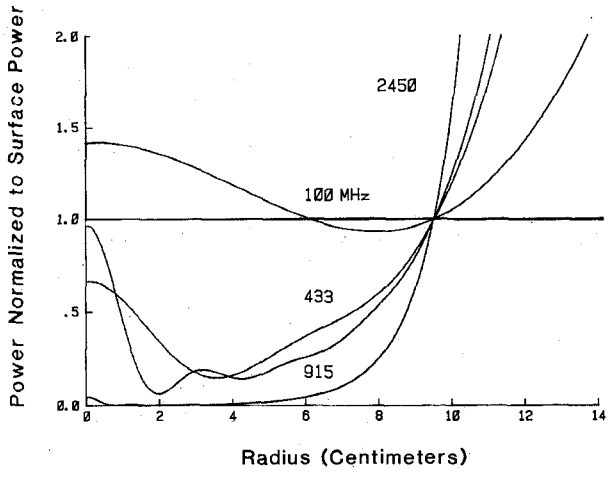

Fig. 6. Power pattern for a 9.5 cm radius sphere of muscle tissue, normalized to the power at the surface.

the poles of the sphere, where the first-order terms vanish and the second-order terms dominate).

The power profiles of Figs. 2 and 5 help determine the maximum safely heated radii for a given frequency. Fig. 6 plots the same power curves normalized to the power on the surface at a fixed radius of 9.5 cm. Note the superiority of the 915 MHz curve both in penetration and resolution.

IV. Conclusions

The preceding discussion has determined the dimensions of the largest convex volume of muscle tissue which can be efficiently heated noninvasively. Constraints have been imposed such that as much power is deposited in the center as elsewhere in the volume or on its surface. These limits are the theoretical best cases (within 1.5 percent): it is not possible to improve on them by altering the surface phase or amplitude distribution. For any other tissue geometry, the maximum penetration depth from surface to center will, of course, be lower. Although the determination of heating patterns depends on the thermal characteristics of the tissue and is governed by the bio-heat equation, it is reasonable to assume that this solution is also the best for heating the center without overheating any intervening tissue. Heating pattern improvements are possible by making use of surface cooling, but this effect is limited to a few millimeters at most.

The novel aspect of this problem is consideration of the vector nature of the source. For scalar waves, such as acoustic waves, the uniform surface excitation would be optimal. For electromagnetic waves, however, polarization is an essential consideration. The method of adding additional higher order modes, which do not contribute to power in the center, to the uniform current distribution simultaneously provides for adjustments to amplitude, phase, and polarization of the source.

Although penetration depth increases with decreasing frequency below 433 MHz., the resolution of the focal spot at the center decreases. However, due to the nonlinear dependence of complex dielectric constant on frequency, increasing the frequency does yield an increase in penetration depth for a limited range, as shown by the plot of 915 MHz power curves. For 433 MHz $\alpha/\beta = 0.396$, whereas for 915 MHz it is 0.231, so the attenuation rate per wavelength is greater for the lower frequency. There is a small advantage to using a more uniform power surface distribution than the uniform current distribution. The improvements are more pronounced for the lower frequencies, since wavelengths are longer and the slopes of the power curves are shallower. It is clear that for muscle tissue geometries of less than 9.5 cm radius, 915 MHz is the best standard frequency for producing a well-focused, high-resolution power peak.

References

[1] G. M. Hahn, *Hyperthermia and Cancer*. New York: Plenum, 1982.
[2] J. G. Short, and P. F. Turner, "Physical hyperthermia and cancer therapy," *Proc. IEEE*, vol. 68, pp. 133–142, Jan. 1980.
[3] C. C. Johnson, and A. W. Guy, "Nonionizing electromagnetic wave effects in biological materials and systems," *Proc. IEEE*, vol. 60, pp. 692–718, June 1972.
[4] R. J. Spiegel, "A review of numerical models for predicting the energy deposition and resultant thermal response of humans exposed to electromagnetic fields," *IEEE Trans. Microwave Theory Tech.*, vol. MTT-32, pp. 730–746, Aug. 1984.
[5] C. M. Weil, "Absorption characteristics of multilayered sphere models exposed to UHF/microwave radiation," *IEEE Trans. Biomed. Eng.*, vol. BME-22, no. 6, pp. 468–476, Nov. 1975.
[6] H. N. Kritikos and H. P. Schwan, "Hot spots generated in conducting spheres by electromagnetic waves and biological implications," *IEEE Trans. Biomed. Eng.*, vol. BME-19, no. 1, pp. 53–58, Jan. 1972.
[7] J. A. Kong, *Electromagnetic Wave Theory*. New York: Wiley, 1986, p. 229.
[8] C. M. Rappaport, and F. R. Morgenthaler, "Localized hyperthermia with EM arrays and the leaky-wave troughguide applicator," *IEEE Trans. Microwave Theory Tech.*, vol. MTT-34, pp. 636–643, May 1986.
[9] J. A. Stratton, *Electromagnetic Theory*. New York: McGraw-Hill, 1941, p. 416.

Carey M. Rappaport (S'81–M'87) received the S.B. degree in mathematics and the S.B., S.M., and Engineers degrees in electrical engineering, all in 1982, and the Ph.D. degree in electrical engineering in 1987, from the Massachusetts Institute of Technology, Cambridge.

He is an Assistant Professor of Electrical Engineering at Northeastern University in Boston, MA. From 1978 until 1983, he spent summers working cooperatively at COMSAT Laboratories in Clarksburg, MD. His research involved reflector antenna measurements, bootlace lens optimization, and computer simulation of spacecraft antennas. During 1984, Dr. Rappaport examined sparsely filled array antenna grating lobe reduction at the Aerospace Corp. in El Segundo, CA. Since 1981, he has served as a teaching assistant and research assistant for MIT's Department of Electrical Engineering and Computer Science. His current research interests involve specialized microwave antenna design for biological and communications applications.

Dr. Rappaport is a member of the Eta Kappa Nu and Sigma Xi honorary professional societies.

Frederic R. Morgenthaler (S'55–M'57–SM'76–F'78) received the S.B. and S.M. degrees in electrical engineering in June 1956 and the Ph.D. degree in June 1960, all from the Massachusetts Institute of Technology.

He is a Professor of Electrical Engineering at MIT. During the academic years 1960 to 1962, he was a Ford Foundation Postdoctoral Fellow in Engineering and an Assistant Professor in the MIT Department of Electrical Engineering. In 1965, he was promoted to the rank of Associate Professor and in 1968 to the rank of Professor. A member of the Research Laboratory of Electronics, the Center for Material Science and Engineering, and Director of the Microwave and Quantum Magnetics Group, he also holds an appointment to the Harvard–MIT Division of Health Sciences and Technology. His research and graduate teaching have centered on the fields of microwave magnetics and ultrasonics, the electrodynamics of waves and media, and microwave signal processing using coherent wave states in solids. He is currently active in the field of magnetic recording. In addition, Dr. Morgenthaler participates in an interdisciplinary course in medical and industrial ultrasonics. He also has taught the undergraduate electrical engineering core curriculum subjects in electromagnetic field theory, circuit theory, and semiconductor electronics. He was in charge of the field theory course from 1965 to 1968 and was lecturer in charge of the transistor course from 1973 to 1978. Dr. Morgenthaler held the Cecil H. Green Professorship for 1984–86. He serves as a consultant to the U.S. Government as well as to private industry.

Dr. Morgenthaler is the author of numerous scientific publications and papers presented at technical conferences and has been granted approximately 12 patents with several others pending. He is a member of the American Physical Society, the American Association for the Advancement of Science, and of the Sigma Xi, Tau Beta Pi, and Eta Kappa Nu honorary professional societies.